RSC Advances

ROYAL SOCIETY OF CHEMISTRY

www.rsc.org/advances

A Table of contents entry:

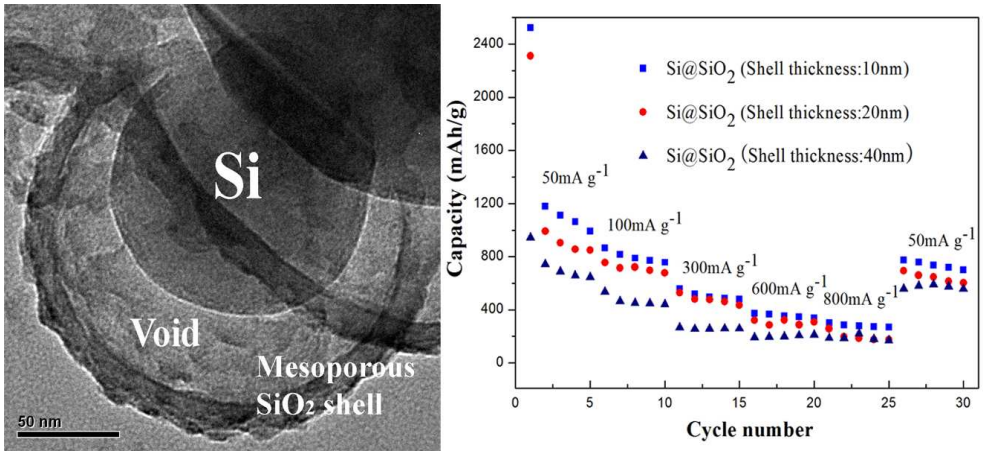

Yolk-mesoporous shell Si@SiO_2 nanohybrids with controllable shell thickness were prepared via a facile vesicle-template method, which exhibit good cycle performance and excellent rate capabilities.

Journal Name

RSCPublishing

ARTICLE

Controlled synthesis of yolk-mesoporous shell Si@SiO_2 nanohybrid designed for high performance Li ion battery

Cite this: DOI: 10.1039/x0xx00000x

Received 00th January 2012,
Accepted 00th January 2012

DOI: 10.1039/x0xx00000x

www.rsc.org/

Zhuang Sun, Xuefeng Song*, Peng Zhang and Lian Gao*

Yolk-mesoporous shell Si@SiO_2 nanohybrid (YMSSN) with void space between the Si core and the SiO_2 outer shell up to tens of nanometers has been prepared in this work by a vesicle template method. Commercially available Si nanoparticles (Nps) are incorporated into mesoporous hollow colloidal SiO_2 spheres (MHSS), which are designed to accommodate large volume change of Si cores and facilitate diffusion of Lithium ions through the pore channels during the lithiation/delithiation process. By adjusting the concentration of surfactants and tetraethyl orthosilicate (TEOS), well-dispersed YMSSN with controllable shell thickness can be obtained. This intriguing structure shows high reversible capacity (~687 mAh g^{-1}), good Coulombic efficiency (95.63 %) and excellent rate-capability.

Introduction

As electric vehicles and consumer electronic devices develop, lithium ion (Li-ion) batteries become one of the most promising energy storage devices owing to their high energy density, long cycle and environment benignity.[1-4] However, graphite, the traditional anode material in Li-ion batteries, was plagued by its limited theoretical specific capacity (~370 mAh g^{-1}), which didn't meet the high energy demands of the advanced electric and hybrid vehicles.[5, 6]

A great deal of anode materials with enhanced storage capacity, high energy density and improved cycle characteristics have been proposed for lithium-ion batteries over the last decade.[7-11] Among all of these candidates, silicon is the most attractive alloy-type anode material because of its highest known capacity (4200 mAh g^{-1}), high volume capacity of 9786 mAh cm^{-3}, and relatively low working potential (0.5 V vs Li/Li^+).[12,13] However, the practical application of Si anodes is severely restricted by the large volume fluctuation. The large volume change (> 300%) during alloying/de-alloying process with lithium not only leads to a loss of electrical contact of Si from current collector due to electrode pulverization, but also makes solid electrolyte interphase (SEI) layer on the surface of Si electrodes unstable, which results in poor rate-capability and short cycle life.[14,15]

Tremendous efforts have been made to circumvent this problem by using nanostructured silicon,[16-20] Si alloy nanohybrids,[21,22] core-shell structured silicon composites.[23,24] Recently, double-walled Si-SiOx nanotubes consisting of an active Si nanotube surrounded by an ion-permeable silicon oxide shell have been reported as promising anode materials, the SiOx outer shell can prevent the electrolyte from wetting the internal Si and result in a stable SEI, which leading to long cycle life and high specific capacity.[25] It should be also noted that the mechanically rigid outer wall SiO_x can prevent the electrolyte from wetting the interior, but the diffusions of Li ions can pass through, which was also confirmed by Zhang et al..[26] Motivated by significant advantages of silicon oxide shell, various nanohybrids have been designed to enhance the performance of Si anodes.[26-29] Despite the progress mentioned above, two impending challenges still need to be addressed. First, in most cases, dense silicon oxide shell was contiguously coated on the Si core. On the one hand, the dense shell was considered not ideal for Lithium diffusion compared with the porous counterpart;[30] On the other hand, the compact structure can't provide sufficient void space to accommodate the huge volume change of Si core. Second, there seems to be lack of well control over Si@SiO_2 composite with rationally defined internal void space such as dispersivity and shell thickness.

Si based "yolk-shell" structure has showed its unique advantages involving to prevent the deposition of SEI on Si surface, avoid the direct contact between Si core and electrolyte solvent, and provide affluent void space to accommodate the huge volume change of Si core.[31-33] Most shells in this special structure are carbon, which allow high electrical conductivity and maintain structural integrity. Nevertheless, the cumbersome procedure and toxic chemicals involved for removing silica template bring high processing cost and environmental concerns. And the dispersivity

of Si@Carbon composites is hard to control due to the indispensable high-temperature carbonization step. To circumvent these problems, a novel YMSSN has been synthesized by a facile vesicle template method for the first time, encapsulating Si cores with mesoporous SiO_2 shell in aqueous media of surfactants (Scheme 1). The unique structure is composed of Si nanoparticle (30~150 nm) as the yolk and uniform mesoporous SiO_2 as the shell. Such a unique LIB electrode structure has the following characteristics. First, the sufficient void space between the Si core and the silica shell allows for the Si cores to expand upon lithiation without breaking the shell. Second, the silica mesoporous shell can facilitate the diffusion of lithium, permit more Li^+ flux across the interface and maintain volume stable associated with the repeated Li^+ insertion/extraction processes, which enhance the rate performance and cycle stability.[30,34,35] Third, the dispersivity of YMSSN and the thickness of silica shell can be readily controlled by adjusting the concentration of surfactants and TEOS, which is crucial to achieve excellent Li^+ insertion/extraction properties. By comparing the electrochemical properties of bare Si and YMSSN with different shell thickness, YMSSN with 10 nm shell exhibit the best cycling stability (687 mAh g^{-1} after 30 cycles) and excellent rate capacity performance.

Experimental Section

Chemicals and reagents: Si Nps (~100 nm, Alfa Aesar), (3-aminopropyl) triethoxysilane ($H_2N(CH_2)_3Si(OC_2H_5)_3$) (APTES, 98%, Alfa Aesar), tetraethyl orthosilicte ($Si(OC_2H_5)_4$) (TEOS, 98%, Sigma - Aldrich), lauryl sulfonate betaine ($CH_3(CH_2)_{11}N^+(CH_3)_2(CH_2)_3SO_3^-$) (LSB, Sigma-Aldrich), sodium dodecyl benzenesulfonate ($C_{18}H_{29}SO_3Na$) (SDBS, > 88%, Na_2SO_4 < 9%, H_2O < 3%, China National Medicines Co. Ltd.), hydrochloric acid (HCl, 36-38%, China National Medicines Co. Ltd.) and acetonitrile (99%, China National Medicines Co. Ltd.) were all purchased and used as received.

Preparation of YMSSN: Lauryl sulfonate betaine (LSB) and sodium dodecyl benzenesulfonate (SDBS) were mixed at 1:1 molar ratio and dissolved in deionized water, followed by magnetic stirring for 1h at room temperature; Then, 10 ml Si colloidal aqueous solution (8~10 g L^{-1}) was added into the surfactant mixture (the concentration of LSB/SDBS:1× 10^{-5} M ~ 5× 10^{-5} M). After vigrous stirring for another 15 min, the resulting solution was heated in water bath at 40 °C, followed by addition of 50 ul 3-aminopropyltriethoxysilane (APTES) and tetraethyl orthosilicate (TEOS) in a certain amount, and then the mixture was stirred for 1 hour. The above suspension was then placed in water bath at 80 °C for another 20 h to ensure complete polymerization of the silica. The resultant product was obtained after centrifugation, washing with ethanol and water, respectively, and then dried in air at 353 K. To remove the surfactant, the obtained solid was dispersed in the acetonitrile solution containing ~35% HCl while vigorously stirring at room temperature for 4 h and then dried at 60 °C for 12 h to obtain the YMSSN.

Characterization: The crystal structure of the as-prepared samples were characterized using powder X-ray diffraction (XRD) on a Goniometer Ultima IV (185 mm) diffractometer with Cu Kα radiation (λ=1.5418 Å) at a step of 0.01° per second. Transmission electron microscopy (TEM) images were achieved on a JEOL JEM-2010F transmission electron microscope operated at an acceleration voltage of 200 kV. Morphologies of as-obtained and cycled products were observed on a field emission scanning electron microscopy (FESEM, FEI Sirion 200). X-ray photoelectron spectroscopic (XPS) measurements were performed on a Kratos AXIS Ultra DLD spectrometer with a monochromatic AlKa X-ray source. Nitrogen absorption and desorption measurements were performed with an Autosorb IQ instrument. The surface areas were calculated by the Brunauer-Emmett-Teller (BET) method, and the pore size distribution was calculated from the adsorption isotherm curves using the density functional theory (DFT) method.

Electrochemical characterization: For preparing working electrodes, a mixture of the samples of YMSSN or pure Si, carbon black, and poly (vinylidene fluoride) (PVDF) at a weight ratio of 1:2:1 was put in N-methyl-2-pyrrolidoner (NMP) solvent to form a slurry, which was then pasted on a copper foil (Shenzhen Kejing Star Technology Co., China). After drying in vacuum at 80 °C, the electrodes were tested in coin cells with Li metal as counter and reference electrodes. The electrolyte was 1M $LiPF_6$ in a mixture solution of ethylene carbonate (EC), diethyl carbonate (DEC) and ethyl methyl carbonate (EMC) in a 1:1:1 volume ratio (Shenzhen Kejing Star Technology Co., China). A microporous membrane (Celgard 2400) was used as the separator. The coin cells were assembled in an argon filled glove box. The galvanostatic charge-discharge tests were conducted in a voltage interval of 0.01 V to 1.5 V using a Bio-Logic VMP-300 Battery Testing System at room temperature. The specific capacity of YMSSN electrode was calculated by using the mass of YMSSN. Electrochemical impedance spectroscopy measurement was carried out over a frequency range from 100 kHz to 10 mHz with an AC signal of 5 mV in amplitude as the perturbation.

Results and Discussion

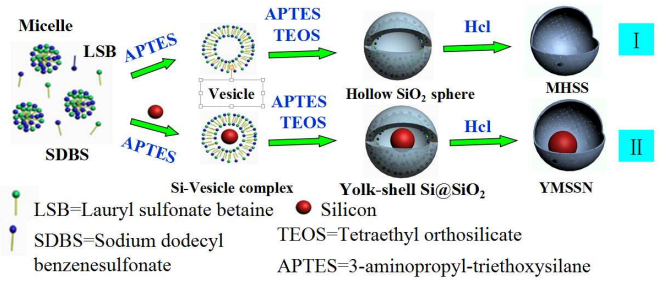

Scheme 1. Schematic procedures for producing YMSSN and MHSS.

The procedure to synthesize YMSSN through a vesicle template method[36] is shown in Scheme 1. Firstly, the spherical micelles consisting of LSB and SDBS were formed at the beginning stage, since the concentration of both surfactants in the mixture was above a certain critical value and single tailed surfactant (including LSB and SDBS) had a packing parameter of less than one-third.[37, 38] Secondly, Si Nps were dispersed into aqueous surfactants mixture with well suspension property; As the vesicle inducing agent APTES was added, the phase transformation from micelles to Si-vesicle complex occurred;[39] Subsequently, a considerable number of amino groups in APTES were protonated and could interact with the negatively charged head groups in the anionic surfactant, the electrostatic attraction between the head groups in surfactants and the amino groups in APTES became a driving force to form the vesicle-silica composite when TEOS was added.[40] Thirdly, the TEOS would hydrolysis and condensation to form a discrete silica layer in the palisade layer of vesicles.[41] After removing the surfactants by HCl, YMSSN could be produced (II). If Si Nps were not added during the second step, micelles would transform to vesicles, and then MHSS could be only produced with the hydrolysis and condensation of silica precursor (I).

TEM analysis was used to investigate the desirable yolk-porous shell structures. Fig. 1a shows the whole morphology of pristine Si Nps with diameter ranging from 30~150 nm, which have a tendency to aggregation. If surfactant, APTES, and TEOS were added without Si Nps during the process, keeping other condition same, MHSS with good dispersivity and mesoporous shell could be obtained, as shown in Fig. 1b. Once Si Nps were added, however, remarkable hollow SiO_2 spheres encapsulating Si Nps could be achieved, as shown in Fig. 1c. Each uniform SiO_2 shell incorporates a few aggregated nanoparticles or one Si nanoparticle. Si Nps are encapsulated in the conformal, porous shell with high encapsulation yield, which is crucial to obtain good electrochemical performance for this YMSSN electrode. Fig. 1d shows a representative single YMSSN, the irregular Si nanoparticle attached tightly with the silica shell by contact points, which can benefit electrons transport from the outer shell to the Si Nps during lithiation.[32] The void space of up to 30~40 nanometers between Si core and thin silica shell can substantially accommodate the volume fluctuation of Si during lithiation/delithiation. Close examination of the YMSSN by scanning electron microscopy (SEM) substantiated that Si Nps were encapsulated by the silica shell (Fig. S1a), and the nanopores can be seen obviously on the surface of the shell (Fig. S1b). The nitrogen adsorption-desorption isotherm for the YMSSN and MHSS prepared here are of typical type IV with a H_3 hysteresis loop at high relative high relative pressure (P/P_0>0.5) (Fig. 1e), confirming the highly mesoporous structure of the silica shell.[42] The corresponding pore size distributions of YMSSN and MHSS are plotted in the Fig. S2 and show similar peaks located at ~3.5 nm using the DFT pore size distribution. The pores can also be confirmed by the the high resolution transmission electron microscopy (HRTEM), in which the mesoporous channels are distributed evenly in the silica shell (Fig. S2c). It is expected that such mesoporous structure will give high BET surface area. They are found to be 121.18 $m^2 g^{-1}$ and 78.99 $m^2 g^{-1}$ for YMSSN and MHSS, respectively. Fig. 1f shows XRD patterns of the Si Nps, MHSS, and YMSSN. It is obvious that the YMSSN has the broad band at around 23° resulted from amorphous silica, the other peaks are identical to that of pure Si Nps which can be readily indexed to cubic Si (JCPDS 65-1060). The silica layer also can be detected by X-ray photoemission spectroscopy (Fig. 2). For bare Si sample, the Si2p spectra demonstrated the presence of silicon oxide peak (Si^{4+}, centered at 103.2 eV) and crystalline silicon (Si^0, centered at 98.9 eV).[43] As Si cores were covered by the SiO_2 shells, XPS survey of YMSSN shows dramatic intensity increase of Si^{4+} peak and apparent intensity decrease of Si^0, suggesting almost all of Si NPs are encapsulated by silica shells in the hybrid.

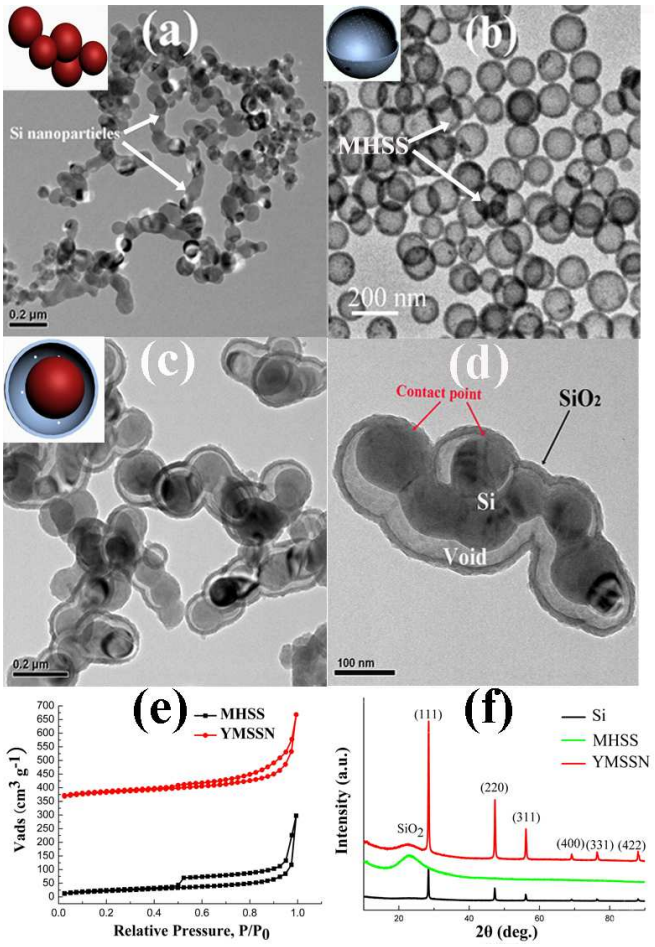

Figure 1. TEM images of a) Si Nps; b) MHSS; (c) YMSSN; d) a single YMSSN; (e) Dinitrogen (N_2) adsorption-desorption isotherms of YMSSN and MHSS; (f) XRD patterns of the Si Nps, MHSS and YMSSN.

The dispersion of YMSSN can be readily controlled by controlling the concentration of LSB/SDBS (Fig. S3). Generally, the hybrids agglomerate severely when the concentration of surfactants is low. The aggregation problem of YMSSN is probably caused by two reasons: one is the severe agglomeration of commercial Si particles which seems hard to eliminate; the other is agglomeration of silica colloids during the hydrolysis and condensation of silica precursor.

To rule out the aggregation effect of Si particles, we only investigated the dispersion of hollow silica. At relatively low

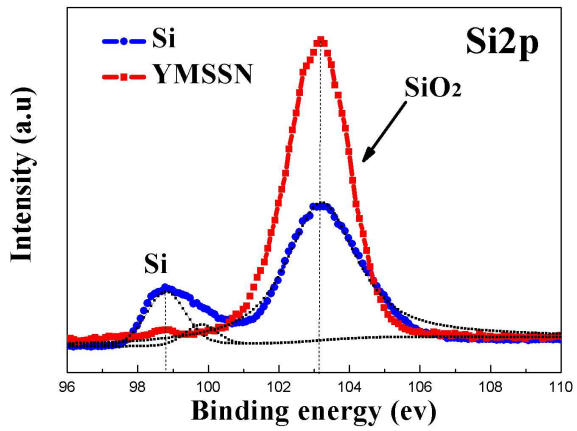

Figure 2. XPS spectra of Si2p on YMSSN and the native Si Nps.

concentration of LSB/SDBS, silica spheres cling to one another to form aggregates (Fig. S3a), which mainly because surfactants are not enough to entirely adsorb on the surface of silica and prevent the aggregation of hollow silica spheres. As the concentration of LSB/SDBS increases to 3×10^{-5} M, the dispersion of spheres is improved (Fig. S3b). When the concentration of LSB/SDBS increases to 5×10^{-5} M, MHSS is well dispersed and isolated MHSS can be obtained (Fig. S3c). At an optimum concentration of LSB/SDBS, plenty of surfactants cover on the surface of hollow SiO_2 colloids, which increase the magnitude of negative zeta potential and steric effects, the dispersivity of hollow SiO_2 colloids are thus improved. Fig. S3d-f show the TEM images of YMSSN with LSB/SDBS concentrations from 1×10^{-5} M to 5×10^{-5} M, in which the dispersion of hybrids are also improved when the concentration of LSB/SDBS increases to optimum concentrations. From the Fig. S3f, YMSSN nanohybrids tend to be apart from each other and most hybrids are isolated. If the amount of surfactants continues to increase, many silica spheres without Si cores will be obtained. Furthermore, in order to systematically elucidate the influence of critical shell thickness on their electrochemical properties, we adjusted the concentration of TEOS and found that the shell thickness can be precisely tuned in the range of 10~40 nm (Fig. S4).

Electrochemical properties of the YMSSN and pristine Si Nps were evaluated in coin cells (CR2025), respectively, and the results are assembled in Fig. 3. Fig. 3a shows typical cyclic voltammetry curves of YMSSN electrode with 10 nm shell thickness in the potential window of 0-1.5 V. For the YMSSN, there are obviously two broad reduction peaks at 0.55-0.8 V and 1.2-1.5 V in the first scanning cycle, respectively, which were observed only in the initial scan and disappeared in the successive scans. The first broad peak (0.55-0.8V) can be attributed to the formation of SEI film on the hybrid anode surface.[29,44] The other broad peak (1.2-1.5V) may be related to the electrochemical reactions between the Li ion and SiO_2 shell to form silicates, which also can be found in bare SiO_2 electrode.[45] Two anodic peaks centered at 0.32 and 0.50 V, gradually evolving from the first scanning cycle and slightly enhancing with the subsequent cycles, corresponding to the delithiation of Li-Si alloy.[44] Subsequent cycles show a lithiation peak at 0.2 V, which corresponds to the reversible Li alloying with active Si to form amorphous Li_xSi phase.[8] Furthermore, the CV curves of YMSSN have very negligible fluctuations from 2nd to 15th cycle. However, the CV curves of Si Nps based anode show obvious fluctuations under the same measure conditions (Fig. S5a), indicating the YMSSN based anode based anode is more stable than the bare Si based anode.

Fig. 3b shows the discharge-charge voltage profiles of the YMSSN for one, two, ten and thirty cycles, respectively. The initial discharge and charge capacities are 2592.9 and 986.4 mAh g^{-1} at a current density of 50 mA g^{-1}, respectively. A long and smooth discharge plateau due to the lithium alloying with crystalline Si was observed in the first discharge. A large irreversible capacity is observed in the first cycle process, which is mostly due to the formation of a SEI layer on the surface SiO_2 shell and the irreversible electrochemical reactions between lithium ions and SiO_2 to form Li_2SiO_3 and Li_4SiO_4.[46] After the first cycle, cycling performances are significantly improved due to the formation of stable SEI layers on the silica shell surface.[45] The discharge capacity is 1068.5 mAh g^{-1} at the second cycle and can be retained at ~687 mAh g^{-1} after 30 cycles, corresponding to a capacity retention of ~64 % compared to that of the second cycle (Fig. 3c), which is higher than that of YMSSN with thicker sheath (YMSSN with 20 nm shell: ~598 mAh g^{-1}, ~56 %; YMSSN with 40 nm shell: ~484 mAh g^{-1}, ~52%). The most likely reason is that the thinner SiO_2 shell reacted with less Li ions resulting in less irreversible capacity loss. Furthermore, it is noteworthy that the average Coulombic efficiency of YMSSN, from 10 to 30 cycles, is as high as 95.63 %, owing to that the affluent void space in the YMSSN can accommodate the huge volume change of Si core and guarantee the structure stability. For comparison, bare Si Nps electrode and Si@silica composites with dense shell electrode (Si Nps were calcined in ambient air at 500° for 2 h to form a solid silica layer coating on the surface, Fig. S5c) were also tested under the same conditions. The Si Nps electrode has a higher initial capacity of 2658 mAh g^{-1}, but dropped rapidly during the subsequent cycles (Fig. S5b). The Si@silica composites with dense shell electrode has a lowest initial capacity (1049 mAh g^{-1}) and only maintains 312 mAh g^{-1} after five cycles (Fig. S5d). Therefore, our design and synthesis of the yolk-porous shell structure is much better and is an effective framework for Si Nps-based anodes.

Fig. 3d shows the rate capability of the YMSSN with 10 ~ 40 nm shell thickness at various rates. For YMSSN with 10 nm shell, the reversible capacities at current densities 50, 100, 300, 600 and 800 mA g^{-1} are ~991, ~867, ~556, ~408 and ~305 mAh g^{-1}, respectively. Even at high current of 600 mA g^{-1}, it still delivers a

Journal Name RSCPublishing

ARTICLE

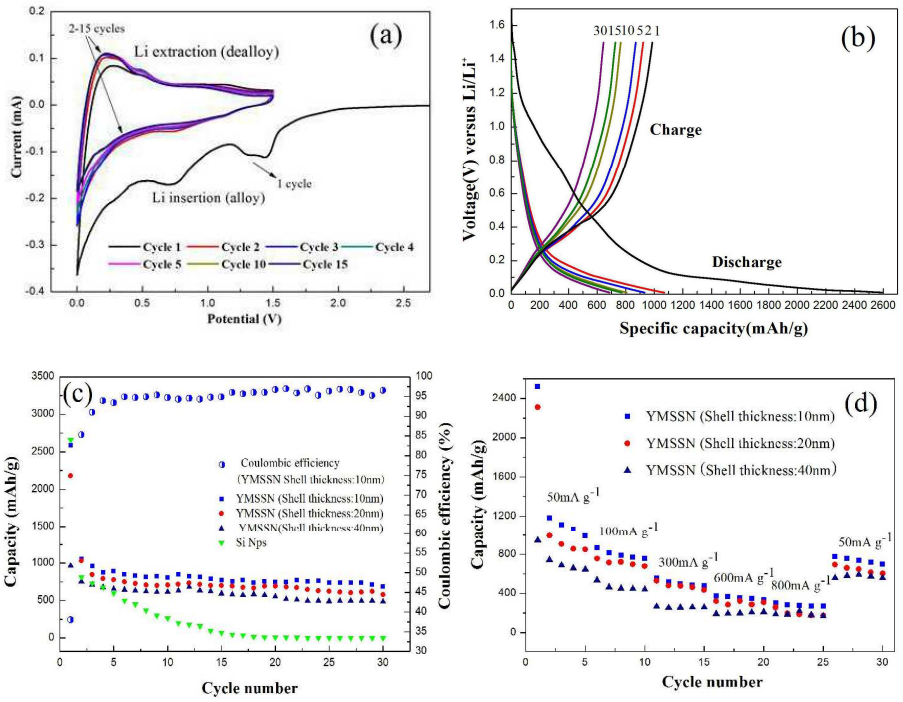

Figure 3. a) Cyclic voltammetry curve of the YMSSN with 10 nm shell thickness showing the first fifteen cycles between 1.5 V and 0 V at a scan rate of 0.1 mV s^{-1}; b) Galvanostatic charge/discharge curves of YMSSN with 10 nm shell thickness at a current rate of 50 mA g^{-1}; c) Cycle performance of YMSSN with 10 ~ 40 nm shell thickness and Coulombic efficiency of YMSSN with 10 nm shell thickness; d) Rate capability of the YMSSN with 10 ~40 nm shell thickness cycled at various rates from 50 to 800 mA g^{-1}.

capacity of ~408 mAh g^{-1}. Remarkably, a capacity of ~773 mAh g^{-1} is recovered when the discharge current rate returns to 50 mA g^{-1} even after 25 cycles at different current rates. The YMSSN with 20 nm shell also has excellent rate capacity performance (~320 mAh g^{-1} at 600 mA g^{-1}, and ~692 mAh g^{-1} is recovered when the charge current rate returns to 50 mA g^{-1}), but the performance of which is not as good as YMSSN with 10 nm shell. The performance of YMSSN with 40 nm shell is relatively low (~257 mAh g^{-1} at 600 mA g^{-1}, and ~538 mAh g^{-1} is recovered when the current rate returns to 50 mA g^{-1}). For the silica shells in this structure, thicker shell would react with more Li ions and result in larger irreversible capacity loss. Further, the time constant for Li^+ and e^- insertion within the active materials is governed by the formula $t= L^2/D$, where L is the diffusion length. In this structure, the pores in the shell are disordered, it is reasonable that the insertion time for Li ions and electrons may get longer as the shell become thicker. Hence, the rate capability decreases with increasing pore wall thickness. Similar phenomena were also observed for mesoporous β-MnO_2 with 5-8.5 nm wall thickness[30] and hollow core-shell structures of $Li_4Ti_5O_{12}$ with 100-200 nm thick shells[47], both of which shows that the rate capability can be improved with decreasing pore wall thickness.

The electrochemical impedance spectra of the YMSSN and crystalline Si Nps were measured to confirm the enhanced electrochemical properties (Fig. 4). Fig. 4 shows the Nyquist plots of bare Si Nps electrode and YMSSN electrode after 10, 20 and 30 cycling, respectively. The semicircle of pure Si became bigger and bigger, suggesting the formation of thicker SEI layer due to cracking or crumbling of the anodes during charge/discharge cycles (Fig. 4a).[29,48] For the YMSSN electrode, the diameter of EIS increased slowly in the first 20 cycles and then remain quite stable, which may be due to the stable SEI formation on the outer surface of SiO_2 shell (Fig. 4b). To verify this, YMSSN and bare Si Nps, after 30 cycles, were retrieved from the cell and investigated by SEM measurement (Fig. S6). It is obvious that the bare Si Nps merge together to be larger ones with a thick and interconnected SEI after 30 cycles. In contrast, the morphologies of hybrid materials after 30 cycles are still spheres, indicating that the aggregation of the Si Nps is alleviated due to the silica shell and the SEI layer deposition on the hybrid electrode has been suppressed.

Besides, it is believed that the nanopores would be blocked after initial several cycles, which also exists in the Si@carbon composites[32]. During cycles, the SEI would form on the surfaces of silica shells and Si cores at the initial stage, and then keep stable as the channels are filled (Fig. 4c, Schematic Ⅱ). This might be the reason why the diameter of EIS for YMSSN increased gradually in the first several cycles and then remain stable. The channels filled by the SEI layer can easily transport Li ions[49] and isolate the yolk from the electrolyte.

This rationally designed yolk-mesoporous shell Si@SiO_2 nanohybrid has three major advantages that ensure the good electrochemical performance. First, the active Si core is encapsulated by the hollow porous silica shell, which can accommodate volume expansion, enhance the structure stability and guarantee good cycle performance. Second, the ultrathin mesoporous silica shell allows the transmission of Li ions through the mesoporous channels, thus permit more Li ion flux travel across the interface. Moreover, most silicon yolk cores tightly contact the outer shells by contact points, which allows for electrons transport from the ultrathin silica shell to the silicon core during continuous cycles. Furthermore, the internal space and pores in the shell can buffer the structural strain and maintain a stable SEI layer on the outer silica shell. All these features make the YMSSN quite stable and show high performance as anode material for Li ion batteries.

Conclusions

In summary, we have successfully synthesized YMSSN for the first time. The yolk-shell nanohybrids involve Si particles incorporated in a hollow colloidal SiO_2 spheres with uniform and porous shell, which effectively accommodates big volume changes of Si, drastically stabilizes the SEI layers and make easier for the diffusion of Lithium during lithiation/delithiation. The dispersion of YMSSN and the thickness of silica shell can be readily controlled by adjusting the concentration of surfactants and TEOS. By comparing the electrochemical properties of bare Si and YMSSN with different shell thickness, the YMSSN anodes with 10 nm thickness exhibit the best cycling stability and high-rate performance. The above observations, supported by the experimental results, confirm the significant electrochemical properties of YMSSN and their potential as next-generation anode materials for high performance lithium ion batteries.

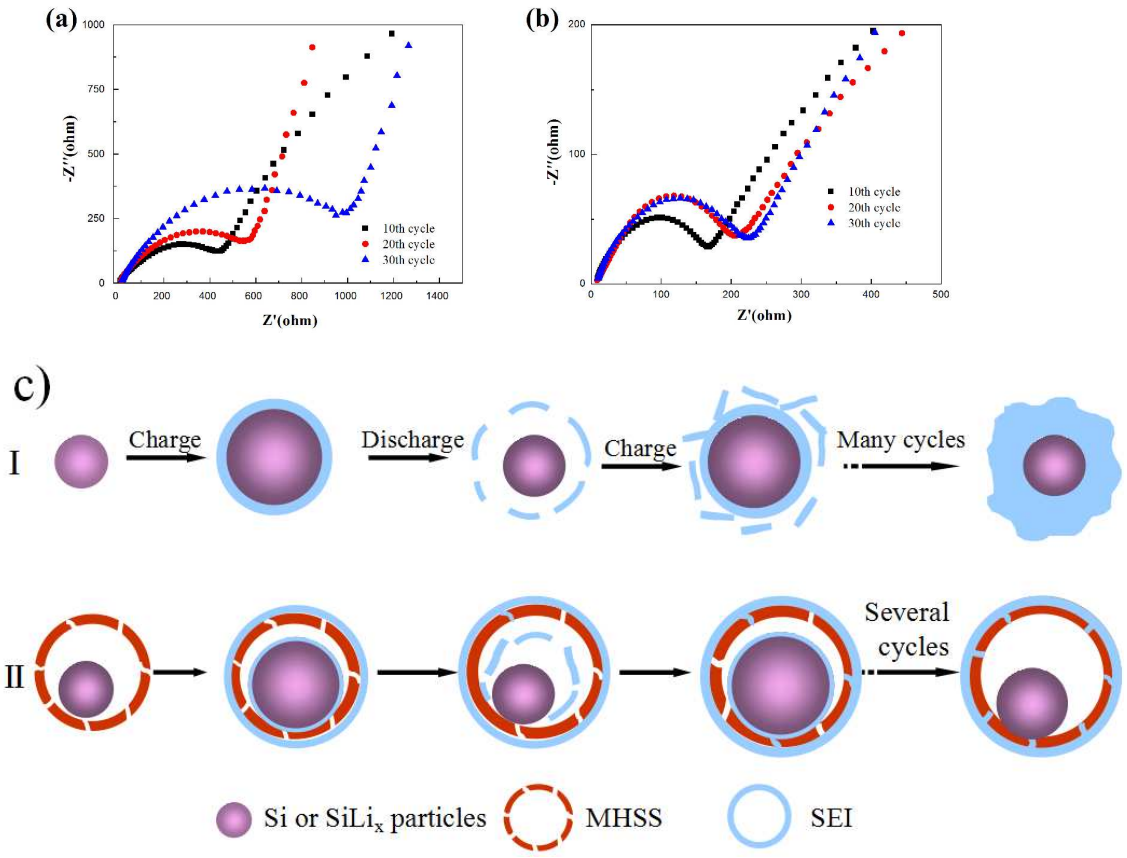

Figure 4. The electrochemical impedance spectra of the a) bare Si Nps and b) YMSSN; c) Schematic of SEI formation for Si Nps (Ⅰ) and YMSSN (Ⅱ) during the lithiation/delithiation process.

Acknowledgements

The authors greatly acknowledge the financial support by the Shanghai Municipal Natural Science Foundation (12ZR1414300), the National Natural Science Foundation of China (51302169, 51172142), the Starting Foundation for New Teacher of Shanghai Jiao Tong University (12X100040119), the Scientific Research Foundation for Returned Overseas Chinese Scholars, State Education Ministry, and the Third Phase of 211 Project for Advanced Materials Science (WS3116205006, WS3116205007).

Notes and references

State Key Lab of Metal Matrix Composites
School of Materials Science and Engineering
Shanghai Jiao Tong University
800 Dongchuan Rd.
Shanghai, P. R. China 200240
E-mail: liangao@mail.sic.ac.cn, songxfeng@sjtu.edu.cn

Electronic Supplementary Information (ESI) available: [More SEM, TEM images of YMSSN and MHSS, electrochemical performances of bare Si Nps and Si@silica composites. See DOI: 10.1039/b000000x/

[1] P. V. Kamat, *J. Phys. Chem. Lett.*, 2011, **2**, 242-251.
[2] P. Johari, Y. Qi and V. B. Shenoy, *Nano Lett.*, 2011, **11**, 5494-5500.
[3] J. O. Besenhard, J. Yang and M. Winter, *J. Power Sources*, 1997, **68**, 87-90.
[4] H. Li, Z. X. Wang, L. Q. Chen and X. J. Huang, *Adv. Mater.*, 2009, **21**, 4593-4607.
[5] H. Wu, G. H. Yu, L. J. Pan, N. Liu, M. T. McDowell, Z. N. Bao and Y. Cui, *Nat. Commun.*, 2013, **4**, 1943-1949.
[6] M. Armand and J. -M. Tarascon, *Nature*, 2008, **451**, 652-657.
[7] L. W. Ji, Z. Lin, M. Alcoutlabi and X. W. Zhang, *Energy Environ. Sci.*, 2011, **4**, 2682-2699.
[8] A. Magasinski, P. Dixon, B. Hertzberg, A. Kvit, J. Ayala and G. Yushin, *Nat. Mater.*, 2010, **9**, 353-358.
[9] C. -M. Park, J. -H. Kim, H. Kim and H. -J. Sohn, *Chem. Soc. Rev.*, 2010, **39**, 3115-3141.
[10] J. M. Yan, H. Z. Huang, J. Zhang, Z. J. Liu and Y. Yang, *J. Power Sources*, 2005, **146**, 264-269.
[11] X. F. Song, *Nanotechnology*, 2013, **24**, 205401-205407.
[12] H. Wu, G. Y. Zheng, N. Liu, T. J. Carney, Y. Yang and Y. Cui, *Nano Lett.*, 2012, **12**, 904-909.
[13] J. R. Szczech and S. Jin, *Energy Environ. Sci.*, 2011, **4**, 56-72.
[14] W. -J. Zhang, *J. Power Sources*, 2011, **196**, 13-24.
[15] H. Wu and Y. Cui, *Nano Today*, 2012, **7**, 414-429.
[16] H. Kim, M. Seo, M. -H. Park and J. Cho, *Angew. Chem. Int. Ed.*, 2010, **49**, 2146-2149.
[17] M. -H. Park, M. G. Kim, J. Joo, K. Kim, J. Kim, S. Ahn, Y. Cui and J. Cho, *Nano Lett.*, 2009, **9**, 3844-3847.
[18] Y. Yao, M. T. McDowell, I. Ryu, H. Wu, N. Liu, L. B. Hu, W. D. Nix and Y. Cui, *Nano Lett.*, 2011, **11**, 2949-2954.
[19] H. Kim, B. Han, J. Choo and J. Cho, *Angew. Chem. Int. Ed.*, 2008, **47**, 10151-10154.
[20] H. Li, X. J. Huang, L. Q. Chen, Z. G. Wu and Y. Liang, *Electrochem. Solid State Lett.*, 1999, **2**, 547-549.
[21] M. D. Fleischauer, J. M. Topple and J. R. Dahn, *Electrochem. Solid State Lett.*, 2005, **8**, A137-A140.
[22] T. D. Hatchard, M. N. Obrovac and J. R. Dahn, *J. Electrochem. Soc.*, 2006, **153**, A282-A287.
[23] P. F. Gao, J. W. Fu, J. Yang, R. G. Lv, J. L. Wang, Y. Nuli and X. Z. Tang, *Phys. Chem. Chem. Phys.*, 2009, **11**, 11101-11105.
[24] L. -F. Cui, R. Ruffo, C. K. Chan, H. L. Peng and Y. Cui, *Nano Lett.*, 2009, **9**, 491-495.
[25] H. Wu, G. Chan, J. W. Choi, I. Ryu, Y. Yao, M. T. McDowell, S. W. Lee, A. Jackson, Y. Yang, L. B. Hu and Y. Cui, *Nat. Nanotechnol.*, 2012, **7**, 310-315.
[26] T. Zhang, J. Gao, H. P. Zhang, L. C. Yang, Y. P. Wu and H. Q. Wu, *Electrochem. commun.*, 2007, **9**, 886-890.
[27] Y. S. Hu, R. Demir-Cakan, M. -M. Titirici, J. -Q. Müller, R. Schlögl, M. Antonietti and J. Maier, *Angew. Chem. Int. Ed.*, 2008, **47**, 1645-1649.
[28] F. Dai, R. Yi, M. L. Gordin, S. R. Chen and D. H. Wang, *Rsc Adv.*, 2012, **2**, 12710-12713.
[29] H. -C. Tao, M. Huang, L. -Z. Fan and X. H. Qu, Solid State Ionics, 2012, **220**, 1-6.
[30] Y. Ren, A. R. Armstrong, F. Jiao and P. G. Bruce, *J. Am. Chem. Soc.*, 2010, 132, 996-1004.
[31] X. L. Li, P. Meduri, X. L. Chen, W. Qi, M. H. Engelhard, W. Xu, F. Ding, J. Xiao, W. Wang, C. M. Wang, J. -G. Zhang and J. Liu, *J. Mater. Chem.*, 2012, **22**, 11014-11017.
[32] N. Liu, H. Wu, M. T. McDowell, Y. Yao, C. M. Wang and Y. Cui, *Nano Lett.*, 2012, **12**, 3315-3321.
[33] Y. C. Ru, D. G. Evans, H. Zhu, and W. S. Yang, *Rsc Adv.*, 2014, **4**, 71-75.
[34] A. Vu, Y. Q. Qian and A. Stein, *Adv. Energy Mater.*, 2012, **2**, 1056-1085.
[35] Y. Zhang, C. Sun, P. Lu, K. Li, S. Song and D. Xue, *CrystEngComm*, 2012, **14**, 5982-5897.
[36] X. -J. Wu and D. S. Xu, *J. Am. Chem. Soc.*, 2009, **131**, 2774-2775.
[37] S. Šegota and Đ. Težak, *Adv. Colloid Interface Sci.*, 2006, **121**, 51-75.
[38] L. M. Zhai, M. Zhao, D. J. Sun, J. C. Hao and L. J. Zhang, *J. Phys. Chem. B*, 2005, **109**, 5627-5630.
[39] X. -J. Wu and D. S. Xu, *Adv. Mater.*, 2010, **22**, 1516-1520.
[40] T. Yokoi, H. Yoshitake, T. Yamada, Y. Kubota and T. Tatsumi, *J. Mater. Chem.*, 2006, **16**, 1125-1135.
[41] J. Yuan, X. T. Bai, M. W. Zhao and L. Q. Zheng, *Langmuir*, 2010, **26**, 11726-11731.
[42] L. X. Zhang, P. C. Li, X. H. Liu, L. W. Du and E. K. Wang, *Adv. Mater.*, 2007, **19**, 4729-4283.

[43] P. Blandin, K. A. Maximova, M. B. Gongalsky, J. F. Sanchez-Royo, V. S. Chirvony, M. Sentis, V. Y. Timoshenko and A. V. Kabashin, *J. Mater. Chem. B*, 2013, **1**, 2489-2495.

[44] S. M. Zhu, C. L. Zhu, J. Ma, Q. Meng, Z. P. Guo, Z. Y. Yu, T. Lu, Y. Li, D. Zhang and W. M. Lau, *Rsc Adv.*, 2013, **3**, 6141-6146.

[45] N. Yan, F. Wang, H. Zhong, Y. Li, Y. Wang, L. Hu and Q. W. Chen, *Sci. Rep.*, 2013, **3**, 1568-1574.

[46] L. W. Su, Z. Zhou and M. M. Ren, *Chem. Commun.*, 2010, **46**, 2590-2592.

[47] C. H. Jiang, Y. Zhou, I. Honma, T. Kudo and H. S. Zhou, *J. Power Sources*, 2007, **166**, 514-518.

[48] Z. P. Guo, J. Z. Wang, H. K. Liu and S. X. Dou, *J. Power Sources*, 2005, **146**, 448-451.

[49] M. B. Prinson and M. Z. Bazant, *J. Electrochem. Soc.*, 2013, **2**, A243-A250.

Keywords

Yolk-shell; Si@SiO_2; Nanohybrids; Lithium ion batteries; Anode material

Zhuang Sun, Xuefeng Song*, Peng Zhang and

Lian Gao*

Title

Controlled synthesis of yolk-mesoporous shell Si@SiO_2 nanohybrid designed for high performance Li ion battery

ToC figure

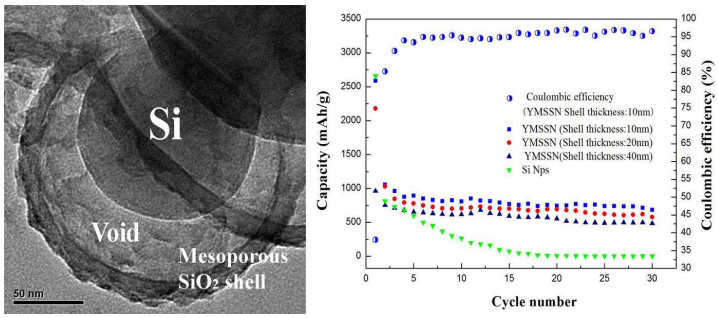

Yolk-mesoporous shell Si@SiO_2 nanohybrids with controllable shell thickness were prepared via a facile vesicle-template method, which exhibit good cycle performance and excellent rate capabilities